nature

THE INTERNATIONAL WEEKLY JOURNAL OF SCIENCE

LIFE FORCE

Did the formation of the Great Unconformity trigger the Cambrian explosion? **PAGE 363**

FRENCH ELECTION

PRESIDENTIAL ADDRESS

The candidates talk science

PAGE 298

PLANETARY SCIENCE

WEATHERING THE STORM

How geomagnetic storms threaten our technologies

PAGE 311

HISTORY

DA VINCI'S ANATOMY

An appreciation of Leonardo the anatomist

PAGE 314

➔ NATURE.COM/NATURE

19 April 2012 $10

$10.00US $12.99CAN

LETTER

doi:10.1038/nature10969

Formation of the 'Great Unconformity' as a trigger for the Cambrian explosion

Shanan E. Peters[1] & Robert R. Gaines[2]

The transition between the Proterozoic and Phanerozoic eons, beginning 542 million years (Myr) ago, is distinguished by the diversification of multicellular animals and by their acquisition of mineralized skeletons during the Cambrian period[1]. Considerable progress has been made in documenting and more precisely correlating biotic patterns in the Neoproterozoic–Cambrian fossil record with geochemical and physical environmental perturbations[2–5], but the mechanisms responsible for those perturbations remain uncertain[1,2]. Here we use new stratigraphic and geochemical data to show that early Palaeozoic marine sediments deposited approximately 540–480 Myr ago record both an expansion in the area of shallow epicontinental seas and anomalous patterns of chemical sedimentation that are indicative of increased oceanic alkalinity and enhanced chemical weathering of continental crust. These geochemical conditions were caused by a protracted period of widespread continental denudation during the Neoproterozoic followed by extensive physical reworking of soil, regolith and basement rock during the first continental-scale marine transgression of the Phanerozoic. The resultant globally occurring stratigraphic surface, which in most regions separates continental crystalline basement rock from much younger Cambrian shallow marine sedimentary deposits, is known as the Great Unconformity[6]. Although Darwin and others have interpreted this widespread hiatus in sedimentation on the continents as a failure of the geologic record, this palaeogeomorphic surface represents a unique physical environmental boundary condition that affected seawater chemistry during a time of profound expansion of shallow marine habitats. Thus, the formation of the Great Unconformity may have been an environmental trigger for the evolution of biomineralization and the 'Cambrian explosion' of ecologic and taxonomic diversity following the Neoproterozoic emergence of animals.

The term Great Unconformity was first used in the year 1869 to describe the prominent stratigraphic surface in the Grand Canyon that separates the shallow marine, ~525-Myr-old Cambrian Tapeats Sandstone from the underlying metamorphosed, 1,740-Myr-old Vishnu Schist and structurally tilted sedimentary rocks of the 1,200–740 Myr-old Grand Canyon Supergroup[6]. The Great Unconformity is well exposed in the Grand Canyon, but this geomorphic surface, which records the erosion and weathering of continental crust followed by sediment accumulation, can be traced across Laurentia and globally, including Gondwana[7,8], Baltica[9], Avalonia[9] and Siberia[10], making it the most widely recognized and distinctive stratigraphic surface in the rock record. It is also notable because the Cambrian sediments that overlie it in many regions preserve the first skeletonized crown-group animals, a fact that some palaeontologists have interpreted as evidence for stratigraphic bias and an incomplete record of early animal evolution[1,6].

Here we use stratigraphic and lithologic data for 21,521 rock units from 830 geographic locations in North America, in conjunction with petrologic and geochemical data (Methods; see also Supplementary Information), to explore the hypothesis that the formation of the Great Unconformity is causally linked to the evolution of biomineralization; this linkage is proposed to occur by means of the geochemical effects of prolonged continental denudation followed by enhanced physical and chemical weathering of continental crust during terminal Ediacaran and Cambrian time.

The Cambrian- to Early Ordovician-aged sediments of the Sauk Sequence[11,12] that overlie the Great Unconformity are time-transgressive, such that Early Cambrian sediments occur on the margins of the palaeocontinents and Late Cambrian sediments overlie the Great Unconformity in continental interiors (Fig. 1). The spatial extent of the Sauk Sequence is comparable to other Phanerozoic continent-scale sedimentary sequences[11,12], but its geological characteristics are unique. In most places, undeformed Cambrian sedimentary rocks deposited on Earth's surface rest non-conformably on much older continental crystalline basement rocks, many of which were formed and/or metamorphosed within the Earth's crust (Fig. 2a). Thus, the Great Unconformity marks the termination of an extended period of continental denudation that exhumed and exposed large areas of igneous and metamorphic rocks to subaerial weathering before marine transgression and subsequent sedimentation.

Continental-scale marine transgression during the Cambrian–Early Ordovician accentuated rates of weathering on the Great Unconformity by shifting landward the position of the erosive transgressive shoreface system, often called the 'wave-base razor'[13], as well as adjacent transitional backshore, aeolian and fluvial systems. As a result, much of the soil and weathered basement rock (regolith) that covered low-relief continental interiors[7] was eroded and mobilized during the transgression, thereby exposing silicate mineral surfaces to weathering over an area that is unprecedented in the rock record (Fig. 2a). This is important because freshly exposed rock weathers chemically at rates more than three times faster than undisturbed soils and regolith[14,15], and

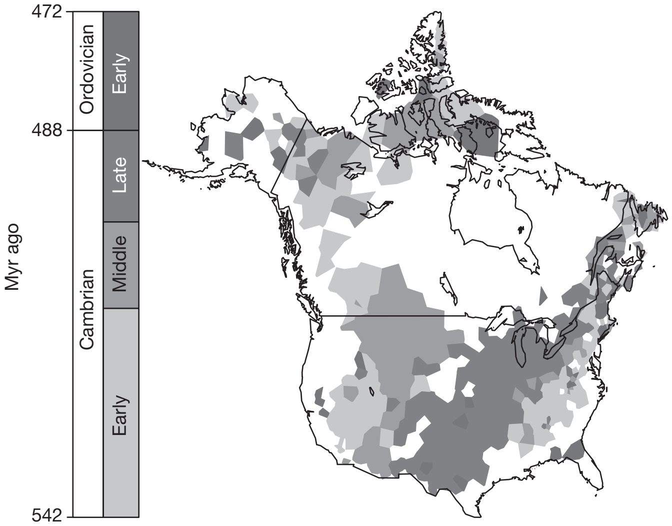

Figure 1 | Sauk Sequence in North America. Distribution and age of the oldest Phanerozoic sedimentary rocks in North America.

[1]Department of Geoscience, University of Wisconsin, Madison, Wisconsin 53706, USA. [2]Geology Department, Pomona College, Claremont, California 91711, USA.

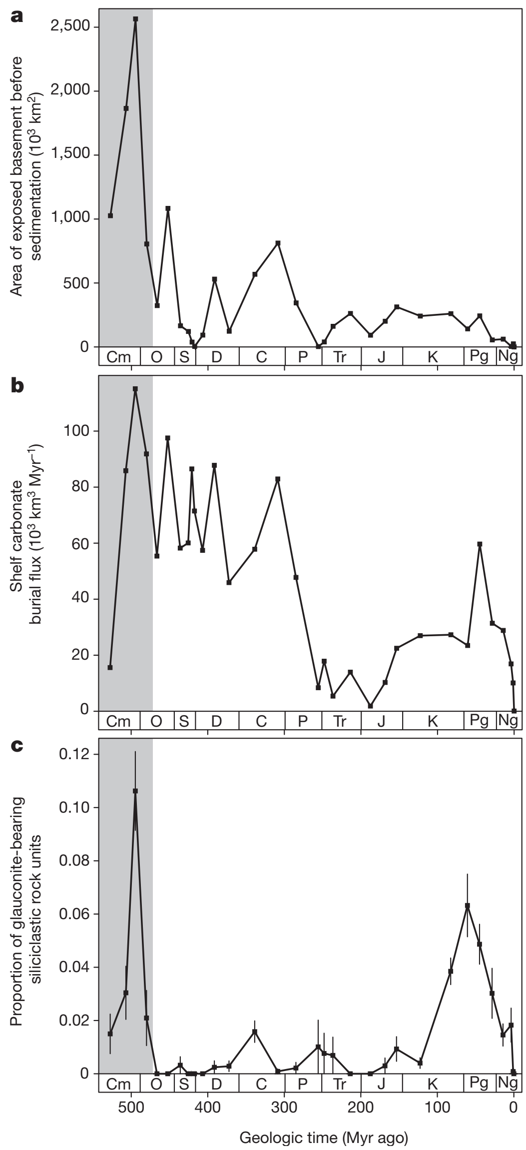

Figure 2 | Phanerozoic sedimentation patterns in North America. **a**, Minimum area of crystalline basement rock exposed at surface before burial by sediments in each epoch. **b**, Estimated minimum total carbonate burial flux in each epoch, based on lithostratigraphic units that are composed primarily of carbonate (Fig. 3c). **c**, Proportion of glauconite-rich siliciclastic sedimentary rock units (Fig. 3d). Grey bars span the Cambrian–Early Ordovician Sauk Sequence. Error bars, ±1 standard error. O, Ordovician; S, Silurian; D, Devonian; C, Carboniferous; P, Permian; Tr, Triassic; J, Jurassic; K, Cretaceous; Pg, Palaeogene; Ng, Neogene.

because the chemical weathering of basement-derived silicate minerals in soils and regolith is enhanced by physical reworking[15]. The sharp stratigraphic contact that typically separates Precambrian basement from the quartz- and feldspar-rich marine sands of the basal, time-transgressive Sauk Sequence (Fig. 3e; see Supplementary Information) demonstrates the efficacy of transgressive shoreface systems in stripping soils and regolith. Shorter-duration eustatic sea level falls, superimposed on the longer-term Sauk transgression, as well as at the terminal Ediacaran[2], provided an additional mechanism for subaerial exposure, reworking and chemical weathering of basement- and regolith-derived sediments.

Exposure and chemical weathering of silicate minerals derived from continental basement rocks during the formation of the Great Unconformity exerted an important control on seawater chemistry and global biogeochemical cycling in several ways, including the consumption of atmospheric CO_2 and the release of HCO_3^-, Ca^{2+}, $H_3SiO_4^-$, SO_4^{2-}, Cl^-, Na^+, Mg^{2+}, K^+, Fe^{3+} and other ions to the oceans[14,15]. We find sedimentological evidence for an increased reservoir size and a sustained flux of continental weathering products to the ocean within each of the three primary facies belts that onlap Cambrian palaeocontinents[16]: the nearshore, generally coarse-grained inner detrital belt, the middle carbonate platform belt, and the outer, fine-grained detrital belt (Fig. 3).

The signal of enhanced continental crustal weathering is perhaps most conspicuously expressed by precipitation of carbonate sediments, which reached a Phanerozoic peak in shelf burial flux during the Sauk transgression (Figs 2b, 3c)[17,18]. In Laurentia, the large quantity of Cambrian–Early Ordovician carbonates is known as the 'Great American Bank'[19]. Precipitation of carbonates is an important sink for alkalinity that is derived from chemical weathering, and we find that the area of continental basement exposed before sedimentation in each time interval (Fig. 2a) is predictive of changes in carbonate burial rates throughout the Phanerozoic (Fig. 2b; partial linear product-moment correlation between first differences, with effect of varying interval duration held constant, is 0.74, $P = 5 \times 10^{-6}$). These results are consistent with a recent model of the Cambrian carbon cycle, which demonstrated that unusually large absolute rates of carbon throughput are required to explain global carbon isotopic excursions[2]. In the absence of a deep-sea sink for carbonate, which did not become established until the Mesozoic origin of calcareous plankton[18,20], Cambrian carbonate burial rates were limited by the rate at which shelf accommodation space was created by sea level rise during the Sauk transgression and by lithospheric subsidence. Thus, it is likely that in the earliest Cambrian ocean there was both a large pre-existing reservoir of chemical weathering products and an enhanced flux originating from the weathering of continental crust.

Additional evidence for an unusually high flux of continental weathering products to the Cambrian ocean, and a corresponding increase in the extent of carbonate precipitation, is provided by petrographic and geochemical data from outer detrital belt mudstones[21]. Although the Phanerozoic rock record is replete with carbonate cemented mudstones, most cements form as a result of microbially mediated remineralization of organic matter and, therefore, have $\delta^{13}C$ values that are significantly depleted relative to sea water[22]. Outer detrital belt mudstones of the Sauk Sequence, by contrast, not only contain a significantly greater wt% carbonate than composite shale standards, but they also yield $\delta^{13}C$ values that are consistent with direct precipitation from sea water (see Supplementary Information). Petrographic analysis reveals that carbonate cements have textures indicative of rapid, displacive growth at bed tops, near the sediment–water interface[21] (Fig. 3b) and that detrital micrite is rare or absent. Furthermore, many outer detrital belt mudstones contain carbonate concretions and/or mud mounds with $\delta^{13}C$ values indicative of precipitation from seawater-derived bicarbonate[23] (see Supplementary Information).

The signal of enhanced weathering of continental crust during the Sauk transgression is evidenced in the inner detrital belt by a peak in the frequency of glauconite-rich siliciclastic rock units (Figs 2c, 3d). Glauconite, $(K,Na)(Fe^{3+},Al,Mg)_2(Si,Al)_4O_{10}(OH)_2$, is a phyllosilicate mineral that in modern marine environments forms at depths of >50 m and in regions where sedimentation rates are low and prolonged periods of pore-water exchange with seawater occur[24]. However, it has been noted that the distribution and abundance of glauconite in Cambrian marine sediments (Fig. 2c) required rapid authigenesis under chemical conditions that are different from those found on modern marine shelves[9,25]. We attribute this anomaly in glauconite formation to an unusually large flux of continental chemical weathering products, particularly K^+, Fe^{3+} and $H_3SiO_4^-$, during the formation of the Great Unconformity. Restricted circulation and low net rates of sedimentation within the inner detrital belt may have also contributed to the unusual distribution and abundance of glauconite.

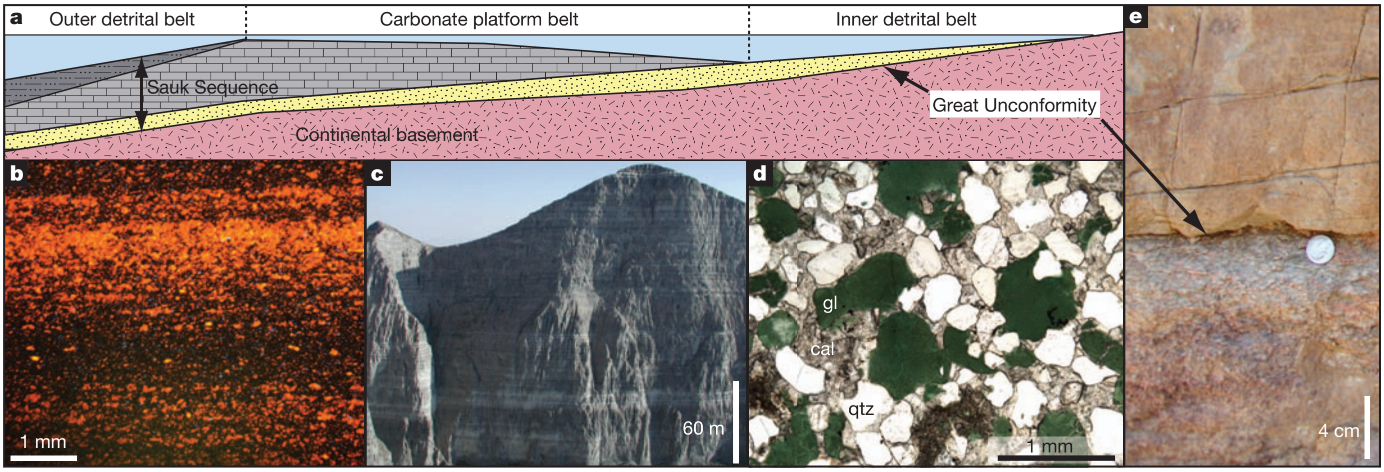

Figure 3 | Middle to Late Cambrian palaeoenvironments and sedimentology. **c**, Generalized marine shelf profile[16]. **b**, Cathodoluminescence photomicrograph of the Kaili Formation, an outer detrital belt mudstone from south China. Lamination tops are defined by authigenic carbonate cements that glow orange under cathodoluminescence; clay-rich lamina bases are dark. **c**, Exposure of Notch Peak Formation in Utah. **d**, Plane-polarized light photomicrograph of a carbonate-cemented, glauconite-bearing sandstone from the Au Train Formation, inner detrital belt, northern Michigan. **e**, Great Unconformity in Wind River Canyon, Wyoming, with ~510- Myr-old marine Flathead Sandstone on 2,900-Myr-old granitic basement. Coin is US dime (17.9 mm diameter). gl, glauconite; cal, calcite; qtz, quartz.

Other records of seawater chemistry provide supporting evidence for changes in tectonic activity and enhanced continental weathering during the formation of the Great Unconformity. For example, the average $^{87}Sr/^{86}Sr$ of sea water increased during the Neoproterozoic (Fig. 4). This long-term signal is attributable to the increasing concentration of ^{87}Sr in continental crust due to the decay of ^{87}Rb, and to the long-term erosion and progressive exposure of ^{87}Sr-rich granitic rocks required to form the Great Unconformity. During the Cambrian, $^{87}Sr/^{86}Sr$ increased more rapidly to achieve a 900 Myr maximum (that is, a maximum over the past 900 Myr) near the end of the Sauk transgression[2], a signal we attribute to enhanced weathering of continental crust during the Sauk transgression. Although Phanerozoic $^{87}Sr/^{86}Sr$ values exhibit many shorter-term oscillations, average $^{87}Sr/^{86}Sr$ values declined after the Late Cambrian peak for most of the Phanerozoic (Fig. 4). We hypothesize that this reversal in the long-term trend in seawater $^{87}Sr/^{86}Sr$ was driven by progressive Phanerozoic sedimentary re-covering of ^{87}Sr-rich continental crust and by increased contributions of ^{86}Sr from the hydrothermal alteration of mid-ocean-ridge basalt. The 900 Myr Cambrian peak in $^{87}Sr/^{86}Sr$ was not approached again until the recent, possibly indicating enhanced removal of Phanerozoic sedimentary cover during Cenozoic orogenesis and global climate change[15].

Congruent evidence for enhanced weathering of continental crust during the Sauk transgression is provided by εNd, an isotopic tracer with a short oceanic residence time that is sensitive to the mean age of continental crust undergoing chemical weathering. Average seawater εNd declined through the Cambrian to reach a long-term minimum at the peak of the Sauk transgression[26] (Fig. 4), reflecting increasingly important input from ancient continental basement rocks as the Sauk transgression progressed from relatively young continental margins into generally older cratonic interiors.

Perhaps the strongest evidence for an increased reservoir and flux of continental chemical weathering products to the global ocean is provided by direct measurements of [Ca^{2+}] in evaporite fluid inclusions. Concentrations of Ca^{2+} in sea water rose precipitously from the Neoproterozoic to reach a Phanerozoic high in the Cambrian[27–29]. We attribute much of this approximately threefold increase in seawater [Ca^{2+}] to enhanced chemical weathering of continental crust during the Sauk transgression. Elevated seawater [Ca^{2+}] has been proposed as a mechanism for the origin of biocalcification by promoting intracellular

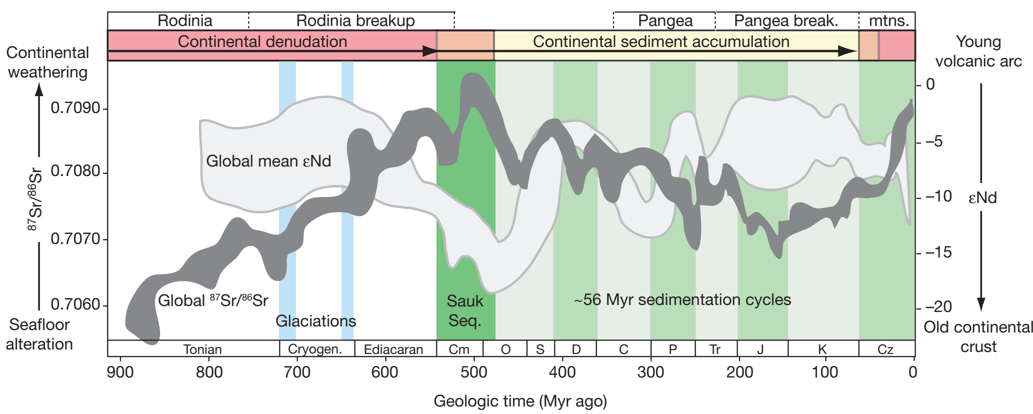

Figure 4 | Summary of major tectonic, geochemical and sedimentary patterns over the past 900 Myr. The shift from widespread continental denudation to widespread sedimentation on the continents defines the Great Unconformity. $^{87}Sr/^{86}Sr$ estimates (dark grey envelope) from ref. 2 and references therein; εNd estimates (light grey envelope) from ref. 26. Vertical blue bars indicate times of major global glaciations; vertical green bars identify continent-scale sedimentary sequences[12], including the Cambrian–Early Ordovician Sauk Sequence (dark green bar). Approximate times of widespread continental denudation are identified by horizontal red bars at top; time of widespread sediment accumulation on continents is identified by partially overlapping light yellow bar. Periods of major supercontinents (Rodinia, Pangea) and their break-up are identified, including recent mountain building (mtns.).

Ca^{2+} concentrations that were toxic to some animals[28,29]. Here we provide a mechanism for this increase in seawater [Ca^{2+}], as well as other ions involved in biomineralization.

The palaeogeomorphic surface represented by the Great Unconformity is unique in at least the past 900 Myr of Earth history, but similar episodes of widespread continental denudation followed by large-scale marine transgression and sedimentation may have occurred before 900 Myr ago. However, the advent of biomineralization and the Cambrian explosion required the presence of animals, which evolved in Cryogenian to Ediacaran time[1,2,30]. Our results therefore offer a new hypothesis for the timing and origin of biomineralization and the Cambrian explosion, both of which lag by tens of millions of years the initial origin of bilaterian animals[30]. Specifically, we propose that biomineralization in multiple clades occurred in response to the changes in global ocean chemistry[28,29] that were promoted by the formation of the Great Unconformity and by the expansion of shallow marine environments that it records. Although Darwin and other palaeontologists have regarded the resultant widespread hiatus in the rock record as a failure of preservation, the formation of this prominent gap may have actually been an environmental trigger for biomineralization, thereby promoting the Cambrian explosion of marine animals[30]. Determining the geodynamic causes of extensive Neoproterozoic continental denudation followed by Phanerozoic sedimentation, and linking those dynamics to the timing and spatial distribution of marine transgression and biogeochemical change, is now a challenge for geoscience.

METHODS SUMMARY

Stratigraphic data derive from Macrostrat (http://macrostrat.org), which consists of 21,521 rock units distributed among 830 geographic regions in North America[30]. Geological ages for the top and bottom of each Phanerozoic rock unit are referenced to one of approximately 82 stage-level time intervals. For this analysis, data were binned into 32 Phanerozoic epochs (median duration 15.6 Myr; see Supplementary Information).

Macrostrat is comprehensive in the sense that all rock units in each region, including those in the subsurface, are included. Rock units have an explicitly identified thickness range and dominant lithology in each region. Many units also have secondary lithologies and, when prominent and characteristic of the unit, additional data on sedimentology, such as mineralogy and sedimentary structures.

To estimate the total number of sedimentary rock packages that directly overlie crystalline basement, all of the rock units older than the base of each Phanerozoic sediment package were tabulated in each region. If there were no older sedimentary rocks at a location, then that package was identified as resting on basement. This approach is conservative with respect to the Great Unconformity because a large fraction of Precambrian sedimentary rock is structurally deformed and laterally adjacent to basement rocks. Thus, the Great Unconformity often cuts across all older rock units at each location[6].

Carbon and oxygen isotopic compositions of 220 outer detrital belt mudstone samples from North America and China were obtained by dissolving whole rock powders in phosphoric acid and analysing evolved CO_2 at the stable isotope laboratories at the University of California Davis and Riverside. Standard errors for all measurements were $\leq 0.2‰$. Whole rock geochemistry measurements from 82 outer detrital belt mudstone samples in North America and China were obtained from ultrasonically cleaned, twice-fused polished glass beads using a Panalytical Axios XRF instrument at Pomona College (see Supplementary Information).

Received 29 June 2011; accepted 16 February 2012.

1. Marshall, C. R. Explaining the Cambrian "Explosion" of animals. Annu. Rev. Earth Planet. Sci. **34,** 355–384 (2006).
2. Maloof, A. C. *et al.* The earliest Cambrian record of animals and ocean geochemical change. Geol. Soc. Am. Bull. **122,** 1731–1774 (2010).
3. Canfield, D. E., Poulton, S. W. & Narbonne, G. M. Late-Neoproterozoic deep-ocean oxygenation and the rise of animal life. Science **315,** 92–95 (2007).
4. Dahl, T. W. *et al.* Devonian rise in atmospheric oxygen correlated to radiations of terrestrial plants and large predatory fish. Proc. Natl Acad. Sci. USA **107,** 17911–17915 (2010).
5. Gill, B. C. *et al.* Geochemical evidence for widespread euxinia in the later Cambrian ocean. Nature **469,** 80–83 (2011).
6. Yochelson, E. L. The Lipalian interval: a forgotten, novel concept in the geologic column. Earth Sci. Hist. **25,** 251–269 (2006).
7. Avigad, D. *et al.* Mass-production of Cambro-Ordovician quartz-rich sandstone as a consequence of chemical weathering of Pan-African terranes: environmental implications. Earth Planet. Sci. Lett. **240,** 818–826 (2005).
8. Laird, M. G. in Geological Evolution of Antarctica (eds Thomson, M. R. A., Crame, J. A. & Thomson, J. W.) 177–186 (Cambridge Univ. Press, 1991).
9. Brasier, M. D. The Lower Cambrian transgression and glauconite-phosphate facies in western Europe. J. Geol. Soc. Lond. **137,** 695–703 (1980).
10. Sears, J. W. & Price, R. A. Tightening the Siberian connection to western Laurentia. Geol. Soc. Am. Bull. **115,** 943–953 (2003).
11. Sloss, L. L. Sequences in the cratonic interior of North America. Geol. Soc. Am. Bull. **74,** 93–114 (1963).
12. Meyers, S. R. & Peters, S. E. A 56 million year rhythm in North American sedimentation during the Phanerozoic. Earth Planet. Sci. Lett. **303,** 174–180 (2011).
13. Cross, T. A. & Lessenger, M. A. in Innovative Applications of Petroleum Technology in the Rocky Mountain Region (eds Coalson, E. B., Osmond, J. C. & Williams, E. T.) 183–203 (Rocky Mountain Association of Geologists, Denver, 1997).
14. Mortatti, J. & Probst, J. Silicate rock weathering and atmospheric/soil CO_2 uptake in the Amazon basin estimated from river water geochemistry: seasonal and spatial variations. Chem. Geol. **197,** 177–196 (2003).
15. Millot, R. Gaillardet, J. Dupré, B. & Allegre, C. J. The global control of silicate weathering rates and the coupling with physical erosion: new insights from rivers of the Canadian Shield. Earth Planet. Sci. Lett. **196,** 83–98 (2002).
16. Robison, R. A. in Guidebook to the Geology of East Central Nevada (eds Boettcher, J. W. Jr & Sloan, W. W.) 43–52 (Intermountain Association of Petroleum Geologists, Salt Lake City, 1960).
17. Ronov, A. B., Khain, V. E., Balukhovsky, A. N. & Seslavinsky, K. B. Quantitative analysis of Phanerozoic sedimentation. Sedim. Geol. **25,** 311–325 (1980).
18. Walker, L. J., Wilkinson, B. H. & Ivany, L. C. Continental drift and Phanerozoic carbonate accumulation in shallow-shelf and deep-marine settings. J. Geol. **110,** 75–87 (2002).
19. Ginsburg, R. N. Actualistic depositional models for the Great American Bank (Cambro-Ordovician). In *Eleventh International Congress on Sedimentology, Abstracts of Papers* 114 (International Association of Sedimentologists/McMaster University, 1982).
20. Ridgwell, A. J., Kennedy, M. J. & Caldeira, K. Carbonate deposition, climate stability, and Neoproterozoic ice ages. Science **302,** 859–862 (2003).
21. Gaines, R. R. *et al.* Mechanism for Burgess Shale-type preservation. Proc. Natl Acad. Sci. USA http://dx.doi.org/10.1073/pnas.1111784109 (published online, 5 March 2012).
22. Coleman, M. L. Geochemistry of diagenetic non-silicate minerals: kinetic considerations. Phil. Trans. R. Soc. Lond. A **315,** 39–56 (1985).
23. Elrick, M. & Snider, A. S. Deep-water stratigraphic cyclicity and carbonate mud mound development in the Middle Cambrian Marjum Formation, House Range, Utah, U.S.A. Sedimentology **49,** 1021–1047 (2002).
24. Odin, G. S. & Matter, A. De glauconiarum origine. Sedimentology **28,** 611–641 (1981).
25. Chafetz, H. S. & Reid, A. Syndepositional shallow-water precipitation of glauconite minerals. Sedim. Geol. **136,** 29–42 (2000).
26. Keto, L. S. & Jacobson, S. B. Nd isotopic variations of Phanerozoic palaeoceans. Earth Planet. Sci. Lett. **90,** 395–410 (1988).
27. Lowenstein, T. K. *et al.* Oscillations in Phanerozoic seawater chemistry: evidence from fluid inclusions. Science **294,** 1086–1088 (2001).
28. Brennan, S. T., Lowenstein, T. K. & Horita, J. Seawater chemistry and the advent of biocalcification. Geology **32,** 473–476 (2004).
29. Petrychenko, O. Y., Peryt, T. M. & Chechei, E. I. Early Cambrian seawater chemistry from fluid inclusions in halite from Siberian evaporites. Chem. Geol. **219,** 149–161 (2005).
30. Erwin, D. H. *et al.* The Cambrian conundrum: early divergence and later ecological success in the early history of animals. Science **334,** 1091–1097 (2011).

Supplementary Information is linked to the online version of the paper at www.nature.com/nature.

Acknowledgements We thank D. Canfield, P. Cohen, W. Fischer, S. Finnegan, N. Heim, A. Carroll and R. Dott for discussion, and N. Butterfield, M. Foote, E. Hammarlund, P. Myrow, B. Wilkinson, R. Wood, S. Holland for feedback on ideas. Fieldwork and analysis was aided by P. Burke, J. B. Caron, L. Curtin, F. Dwan, Z. Feng, P. Fenton, L. Finley-Blasi, X. Hou, J. Lackey, C. Qi, J. Peng, J. Tian, J. Vorhies, Y. Yang, X. Zhang and Y. Zhao. Work was supported by NSF EAR-0819931 (to S.E.P.) and EAR-1046233 and DUE-0942447 (to R.R.G.).

Author Contributions S.E.P. contributed Macrostrat-derived data, R.R.G. contributed sample-derived data. Both authors contributed to the development of ideas and writing.

Author Information Data for aspects of this analysis derive from Macrostrat (http://macrostrat.org). Reprints and permissions information is available at www.nature.com/reprints. The authors declare no competing financial interests. Readers are welcome to comment on the online version of this article at www.nature.com/nature. Correspondence and requests for materials should be addressed to S.E.P. (peters@geology.wisc.edu).

doi:10.1038/nature10969

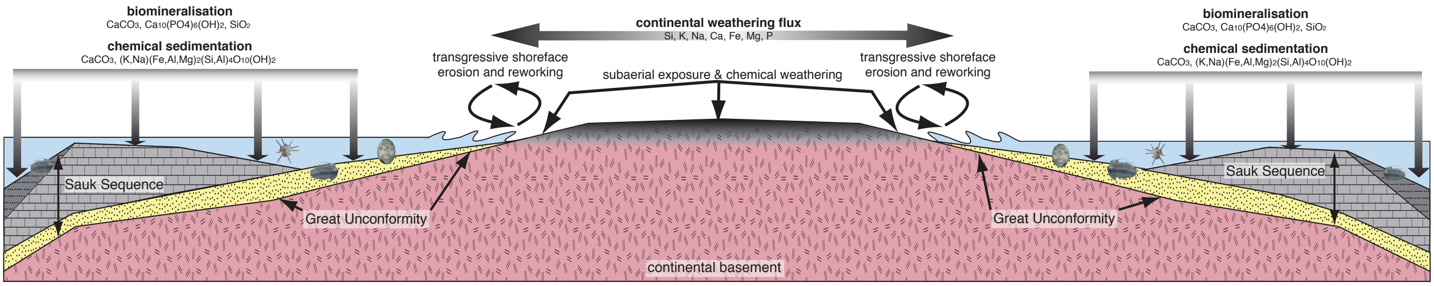

Figure S1. Schematic diagram of major surface conditions and processes during the formation of the Great Unconformity. Large portions of many paleocontinents were exposed to subaerial weathering during the Precambrian, resulting in widespread denudation and weathering of continental crust. Marine transgression during the Cambrian caused the erosion and mobilisation of regolith and soils in shoreface and upslope environments, resulting in an enhanced flux of chemical weathering products to the ocean. Superimposed shorter-duration sea level falls contributed to enhanced weathering of mobilsed soil and regolith. Transgressive Cambrian shallow marine sediments onlap physically eroded basement rocks, thereby preserving the geomorphic surface represented by the Great Unconformity. The chemical weathering products derived from weathering of continental crust were deposited as carbonate rock in many shelf environments and as glauconite in shallow nearshore environments, and both of these chemical sediments occur with unusual abundance and environmental distribution in the Cambrian. Enhanced weathering flux also promoted the origin of biomineralisation, utilising calcium carbonate, apatite, and silicon dioxide, in multiple lineages that had evolved millions of years prior.

Figure S2. Macrostrat coverage area. Geographic distribution and estimated areas for each of the 830 columns in Macrostrat that were used for all analyses. Central America and the Caribbean lack Early Paleozoic sediments and are, therefore, not shown in text Fig. 1.

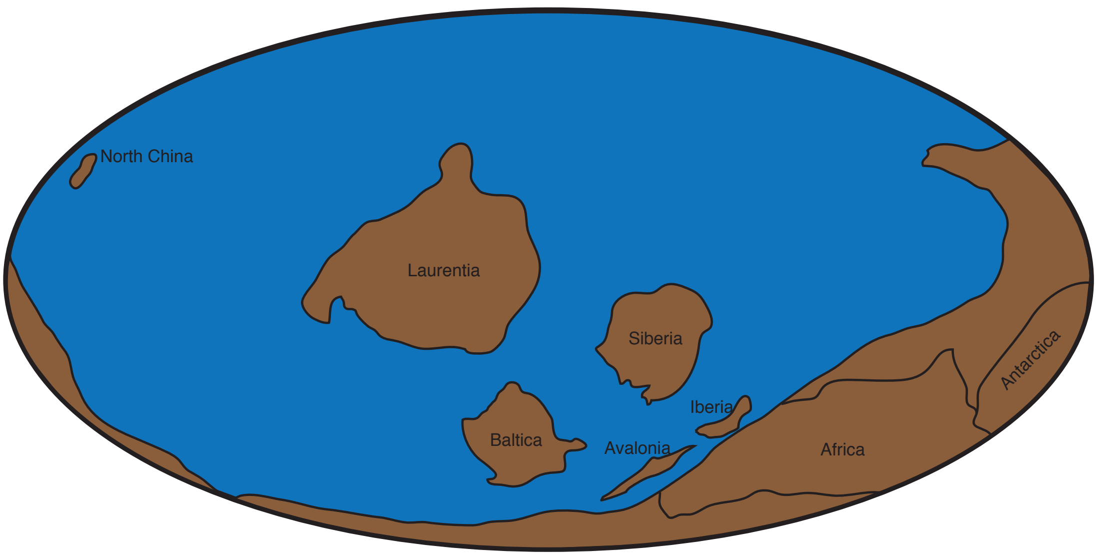

Figure S3. A possible paleogeographic reconstruction for the Late Cambrian. (after reconstruction from Scotese.com). The supercontinent over the south pole is Gondwana, the locations of selected and continental blocks cratons are marked. The GUn is present on all paleocontinents, with Sauk-aged sediments onlapping basement rock in Laurentia (data provided in this study), Baltica (Brasier, 1980; Miller et al., 2011), Gondwana (Africa: Avigad et al., 2005; Antarctica: Laird, 1998), Siberia (Sears and Price, 2003), North China (Meng et al., 1997), Iberia (Liñán et al., 2002), and Avalonia (Brasier, 1980), among other locations.

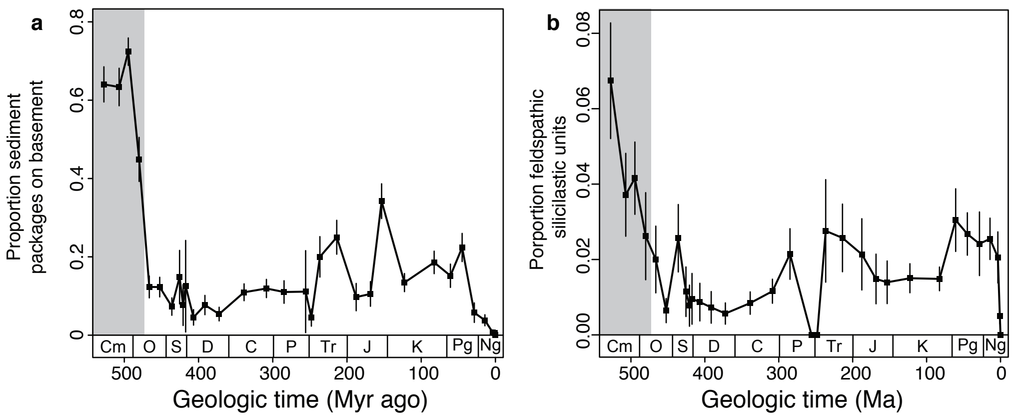

Figure S4. Macrostratigraphic and lithologic variability in the Phanerozoic. a, Proportion of Macrostrat columns (as identified if Fig. S1) with packages initiating in each epoch and that rest on crystalline basement rock. Compare to text Fig. 2a. **b,** Proportion of all siliciclastic sedimentary rock units that are identified as feldspar-rich in Macrostrat. The Cambrian high in this trend illustrates the predominance of basement rock sediment sources at this time. Compilations of whole rock geochemical data from feldspar rich sandstones show strongly elevated SiO_2 concentrations (avg. 78.7%; Pettijohn et al., 1987) vs. average bulk continental crust (57.3%; Taylor and McLennan, 1985) and thus imply significant, although incomplete chemical weathering of parent material. Error bars are ± 1 standard error. Gray band spans the duration of the Sauk Sequence.

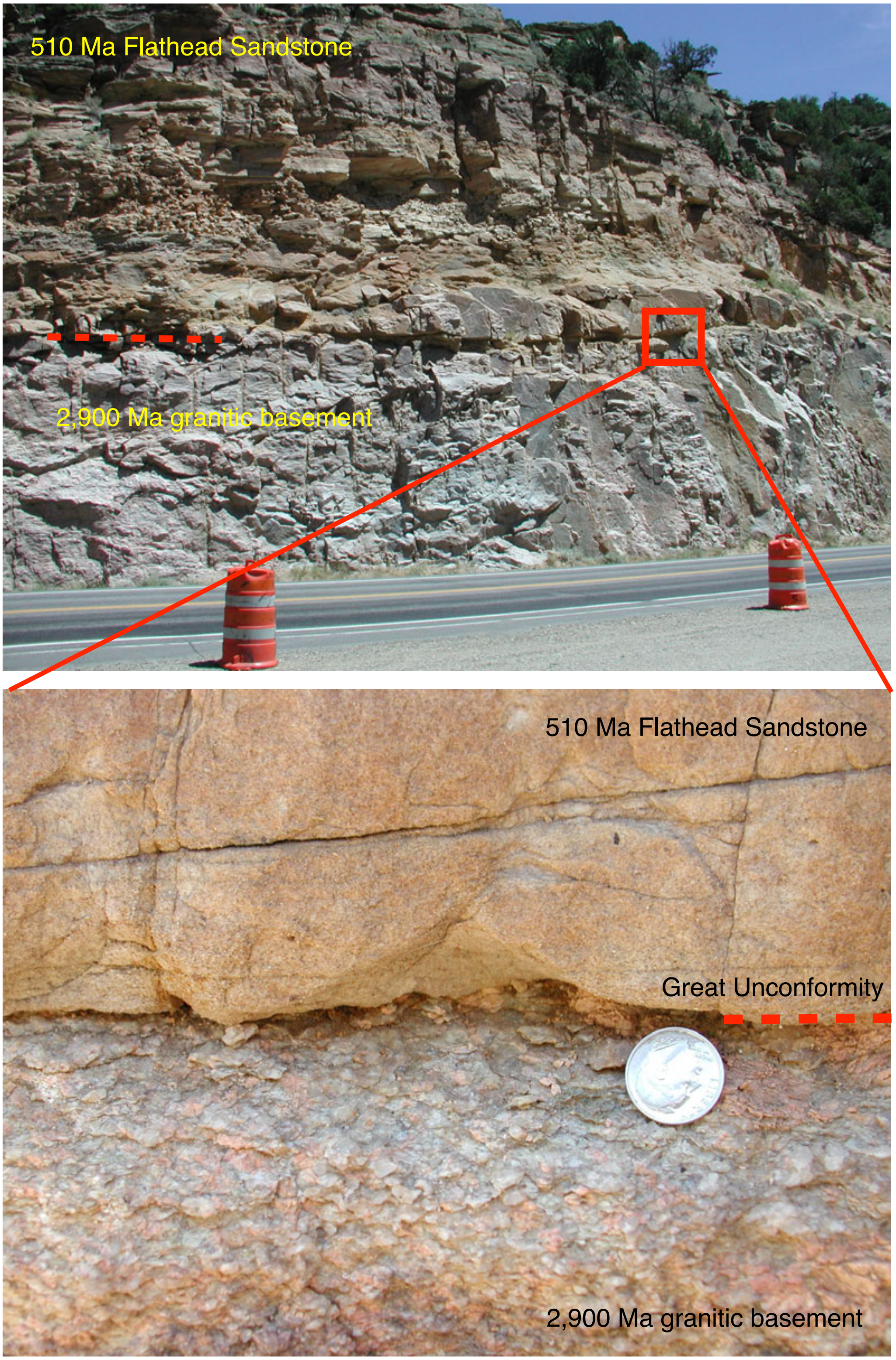

Figure S5. The Great Unconformity. Exposures of GUn (dashed lines) in Wind River Canyon, Wyoming. The Flathead Sandstone was deposited in a transgressive marine shoreface environment. Note the lack of soils or deep weathering on granitic basement. This is typical of the GUn in North America, which can be traced from California to New York. Ma, millions of years ago. U.S.A. dime, 17.9 mm.

Figure S6. The Great Unconformity. Cut section, from 2,176.8 feet depth, of core UPH-3, ISGS number C12996, from the subsurface of northern Illinois (42.4373 N, 89.8578 W). Note the sharp contact between crystalline basement rock and arkosic sands of overlying Late Cambrian Mount Simon Sandstone. Although the basement rock is somewhat chemically altered, there is no well-developed regolith or soil profile; it is possible that all of the alteration took place during burial diagenesis as ground water readily circulated through the permeable Mt. Simon and impinged on relatively impermeable basement.

Figure S7. The Great Unconformity. Exposure of GUn (red dashed line) outside of Manitou Springs, CO. The GUn was rotated from the horizontal during more recent Laramide deformation.

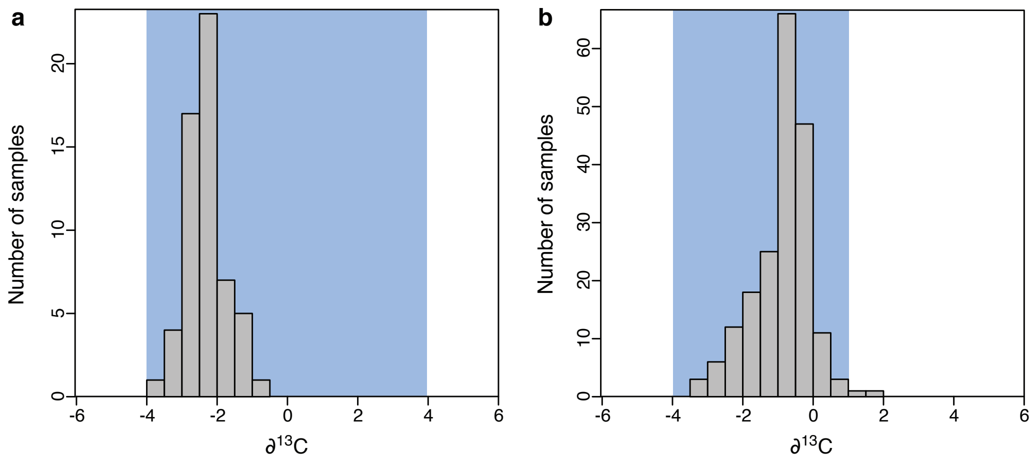

Figure S8. Carbon isotopic composition of outer detrital belt mudstones. a. Frequency distribution of $\partial^{13}C$ values of authigenic cements and concretions of Early Cambrian age. **b.** Frequency distribution of $\partial^{13}C$ values of authigenic cements and concretions of Middle Cambrian age. The approximate range of seawater values for each of these time intervals is shown by blue fields (data from Maloof et al., 2010 and Montañez et al., 2000). Analytical methods, samples and values are reported in Table S2 below.

Table S1: Carbonate content of outer detrital belt mudstones. XRF major element geochemistry of 108 mudstone samples from six Early to Late Cambrian mudstone-dominated stratigraphic units of the outer detrital belt of North America and south China. Samples were powdered using a Rocklabs shatterbox fitted with a tungsten carbide grinding head. 3.5g of whole rock powders were mixed with 7.0g of a lithium tetraborate flux and fused in graphite crucibles at 1000˚C for ten minutes and cooled at room temperature to form glass beads. Glass beads were then re-powdered and fused a second time at 1000˚C. Following the second fusion, glass beads were polished, cleaned by ultrasound, and analyzed for major and minor element chemistry using a Panalytical Axios XRF instrument at Pomona College. The PAAS (Post-Archean Australian Shale standard; Taylor & McLennan, 1985), a widely used composite standard, is shown for reference. Of particular note is the elevated CaO of these mudstone samples (avg. 6.75 wt.%) relative to the PAAS average (1.30 wt.%), a consequence of higher wt. % carbonate in these samples vs. the composite average. Carbonate is readily lost to surface weathering (as in samples MH5 0.30 – 0.62) and reduced during metamorphism (as in samples SG 27.62- 30.00), so measured values likely under estimate true abundance. Diminished wt.% SiO_2, Al_2O_3 and Fe_2O_3 of the sample set vs. the PAAS standard also results from dilution by carbonate. Samples were prepared for XRF analysis as fused glass beads following the method of (Johnson et al., 1999). Stephen Formation samples belong to Royal Ontario Museum collections # 59951 and # 10-045.

Unit	Sample	SiO_2 (wt. %)	TiO_2 (wt. %)	Al_2O_3 (wt. %)	Fe_2O_3 (wt. %)	MgO (wt. %)	MnO (wt. %)	CaO (wt. %)	K_2O (wt. %)	Na_2O (wt. %)	P_2O_5 (wt. %)
Balang Formation											
	CBN1	51.02	0.66	16.18	6.06	3.64	0.05	5.40	4.76	0.61	0.07
	CBN2	54.33	0.61	17.91	6.80	3.21	0.04	2.42	5.15	0.79	0.09
	CBN3	49.11	1.60	18.00	9.78	2.61	0.05	6.67	0.30	3.46	0.35
	CBN4	57.26	1.00	18.23	4.94	2.69	0.07	6.67	0.71	4.22	0.35
	CBN5	58.58	1.02	18.13	5.70	2.93	0.08	6.12	0.71	4.21	0.21
Spence Shale Member (Langston Formation)											
	MH5 0.30	55.60	0.92	25.39	3.79	1.38	0.00	0.13	6.86	0.32	0.13
	MH5 0.38	54.52	0.91	25.04	4.76	1.63	0.01	0.33	6.58	0.30	0.13
	MH5 0.62	56.66	0.93	25.92	2.34	0.83	0.00	0.15	7.35	0.37	0.12
	MH5 0.98	51.38	0.84	23.49	7.75	2.42	0.03	1.53	5.55	0.27	0.12
	MH5 1.21	52.49	0.88	23.75	5.88	1.88	0.03	1.78	5.92	0.27	0.10
	ON1	46.56	0.73	19.28	5.83	2.02	0.06	10.01	3.37	0.78	0.10
Kaili Formation											
	CK 7	30.39	0.33	8.81	2.52	1.19	0.05	27.78	5.02	0.05	0.08
	CK14	24.65	0.23	6.82	2.64	1.33	0.07	33.15	2.66	0.02	0.07
	CK53	52.11	0.7	18.09	8.82	2.95	0.13	2.87	5.31	0.44	0.13
	CKM 74	56.58	0.74	18.5	8.35	3.08	0.13	0.85	4.95	0.74	0.14
	CKM133	34.21	0.45	11.63	5.36	1.79	0.18	21.86	3.19	0.34	0.09
	CKM62	55.13	0.75	18.79	8.89	3.05	0.06	0.43	5.1	0.55	0.13
	CKM65	54.61	0.72	18.58	8.76	3.07	0.12	1.05	5.11	0.55	0.16
	CKM78	52.25	0.68	17.59	7.05	2.82	0.06	0.25	4.65	0.62	0.12
	CKM88	46.4	0.58	15.67	6.34	2.49	0.03	0.26	4	0.57	0.11
Marjum Formation											
	MJ 0.21	42.39	0.53	14.49	5.22	3.33	0.03	14.71	2.53	0.36	0.08
	MJ 0.47	41.60	0.49	13.93	5.55	3.40	0.03	15.39	2.35	0.35	0.07
	MJ 0.68	39.58	0.45	13.09	5.42	3.39	0.03	17.28	2.14	0.33	0.07
	MJ1 0.01	30.45	0.36	9.93	3.69	2.49	0.02	11.29	1.65	0.24	0.05
McKay Group											
	CMK 104	56.13	0.71	19.37	8.27	3.07	0.05	0.17	5.14	0.64	0.12
	CMK 18	43.64	0.56	15.12	5.22	2.97	0.06	14.28	2.41	1.1	0.09

Unit	Sample	SiO_2 (wt. %)	TiO_2 (wt. %)	Al_2O_3 (wt. %)	Fe_2O_3 (wt. %)	MgO (wt. %)	MnO (wt. %)	CaO (wt. %)	K_2O (wt. %)	Na_2O (wt. %)	P_2O_5 (wt. %)
	CMK 3	44.13	0.55	15.06	4.86	2.73	0.06	13.81	2.46	1.03	0.08
	CMK14	45.63	0.58	15.75	4.72	2.75	0.05	12.23	2.63	1.07	0.08
	CMK40	44.65	0.56	15.31	4.74	2.73	0.06	13.15	2.53	1.03	0.08
	CMK50	42.88	0.56	14.69	5.06	2.89	0.06	14.66	2.36	1.03	0.08
Stephen Formation											
	S72A	48.71	0.67	22.61	9.09	3.26	0.03	3.89	2.79	1.05	0.19
	S72B	47.87	0.69	22.31	7.2	2.69	0.04	5.9	2.98	1.13	0.18
	S72C	48.24	0.66	20.31	7.32	2.74	0.04	7.32	2.58	0.98	0.16
	S72D	46.39	0.65	20.56	7.13	2.88	0.05	7.74	2.73	0.95	0.23
	S72E	49.81	0.7	21.94	6.02	2.25	0.04	5.92	3.02	1.17	0.16
	S72F	45.09	0.63	20.04	6.38	2.26	0.09	8.97	2.87	1.14	0.13
	S73A	53.2	0.73	24.6	7.18	2.49	0.03	1.2	3.28	1.3	0.16
	S73B	45.17	0.6	22.22	5.86	2.31	0.01	1.05	2.76	1.2	0.13
	S73C	51.25	0.78	25.74	6.61	2.38	0.02	1.84	3.49	1.38	0.15
	S73D	50.73	0.7	23.01	6.97	2.56	0.03	4.11	3.06	1.18	0.13
	SG1 27.62	52.60	0.73	23.87	6.90	2.22	0.01	1.50	4.51	0.84	0.09
	SG1 28.31	51.46	0.70	23.08	7.59	2.37	0.01	2.02	4.32	0.76	0.10
	SG1 29.65	52.08	0.72	22.60	7.72	2.38	0.02	2.10	4.21	0.77	0.13
	SG1 29.65	52.16	0.72	22.61	7.71	2.37	0.01	2.10	4.20	0.77	0.13
	SG1 30.00	50.56	0.70	22.89	7.92	2.53	0.02	2.56	4.21	0.73	0.09
Wheeler Formation											
	CW SS 1	44.13	0.45	13.78	6.02	4.29	0.06	11.49	2.78	0.67	0.06
	CW SS 2	40.01	0.39	12.06	6.26	4.58	0.04	14.37	2.36	0.64	0.05
	CW SS 3	44.49	0.47	14.06	5.74	4.24	0.06	11.12	2.88	0.68	0.05
	CW SS 1	40.40	0.42	12.27	5.86	4.44	0.06	14.29	2.43	0.66	0.05
	CW SS 1	40.94	0.42	12.47	5.93	4.45	0.04	13.83	2.49	0.63	0.05
	CW WA2	47.36	0.63	17.12	5.90	4.36	0.02	7.44	3.58	0.55	0.07
	CW WA1 A	44.84	0.57	14.96	5.11	4.37	0.04	9.75	3.36	0.59	0.09
	CW WA1 B	48.79	0.64	17.21	5.03	4.24	0.03	6.38	3.79	0.60	0.08
	CW WA1 C	47.86	0.60	16.58	5.07	4.35	0.04	7.26	3.64	0.58	0.09
	CW WA1 D	42.69	0.49	13.53	5.26	4.58	0.04	11.84	2.96	0.58	0.07
	CW WA1 E	41.85	0.51	13.57	5.17	4.56	0.04	12.23	3.05	0.56	0.07
	CW WA1 F	42.38	0.46	13.15	5.66	4.49	0.05	12.68	2.93	0.41	0.07
	CW SSL 1	41.51	0.47	12.43	5.70	4.49	0.05	13.40	2.83	0.40	0.06
	CW WA1 G	37.32	0.40	10.92	5.32	4.80	0.05	16.22	2.36	0.53	0.06
	CW WA1 H	37.53	0.42	10.64	5.91	5.29	0.09	15.05	2.25	0.57	0.08
	CW WA1 I	17.49	0.25	4.79	4.71	5.26	0.05	31.66	1.18	0.30	0.07
	CW SSL 1	38.49	0.38	10.03	5.70	4.68	0.06	16.69	2.20	0.33	0.04
	CW SSL 2	36.91	0.43	11.27	5.63	4.52	0.07	16.28	2.64	0.46	0.06
	CW SSL 3	35.68	0.38	10.14	5.85	4.70	0.05	17.52	2.36	0.36	0.05
Yu'anshan Formation											
	CJ1 12.96E	55.57	0.64	11.32	4.20	5.94	0.07	5.89	3.31	0.19	0.65
	CJ1 15.26E	52.88	0.10	13.75	5.49	5.90	0.08	5.07	3.84	0.19	0.67
	CJ1 15.28B	51.86	0.11	16.74	6.21	5.10	0.06	2.97	4.66	0.18	0.66
	CJ1 21.27B	54.07	0.10	17.38	5.84	4.53	0.05	1.96	4.80	0.22	0.68
	CJ1 22.25B	52.49	0.05	16.78	5.75	5.06	0.06	3.00	4.69	0.25	0.66

Unit	Sample	SiO_2 (wt. %)	TiO_2 (wt. %)	Al_2O_3 (wt. %)	Fe_2O_3 (wt. %)	MgO (wt. %)	MnO (wt. %)	CaO (wt. %)	K_2O (wt. %)	Na_2O (wt. %)	P_2O_5 (wt. %)
	CJ1 23.30E	41.96	0.12	14.17	5.55	7.39	0.13	7.39	3.90	0.20	0.60
	CJ1 23.33B	53.03	0.18	16.32	5.58	5.17	0.06	3.25	4.58	0.19	0.65
	CJ1 23.37B	51.70	0.19	16.86	6.43	5.08	0.06	2.80	4.70	0.19	0.68
	CJ1 23.37E	51.08	0.17	18.14	6.65	5.05	0.06	2.17	4.95	0.21	0.72
	CJ1 23.40E	51.24	0.16	15.81	6.64	5.44	0.07	3.46	4.34	0.21	0.69
	CJ1 23.43B	52.06	0.24	16.84	6.19	5.07	0.06	2.89	4.71	0.20	0.68
	CJ1 23.51B	52.18	0.13	16.13	5.71	5.18	0.06	3.20	4.53	0.20	0.67
	CJ1 23.51E	51.23	0.18	17.77	6.64	5.08	0.06	2.29	4.84	0.21	0.71
	CJ1 23.57E	50.48	0.21	18.20	6.92	4.95	0.06	2.00	4.94	0.21	0.72
	CJ1 23.60B	52.36	0.09	16.63	6.15	5.07	0.06	2.87	4.64	0.20	0.66
	CJ1 23.73B	54.36	0.17	16.39	5.50	4.65	0.05	2.38	4.62	0.19	0.65
	CJ1 23.91B	52.76	0.20	16.71	5.81	5.11	0.06	3.03	4.68	0.20	0.67
	CJ1 24.12B	54.29	0.13	16.31	5.48	4.74	0.06	2.75	4.64	0.24	0.67
	CJ1 24.22B	53.31	0.22	16.49	5.63	4.88	0.09	2.87	4.65	0.24	0.66
	CJ1 24.62B	53.32	0.33	16.51	5.69	5.09	0.06	3.11	4.63	0.24	0.66
	CJ1 24.70B	52.35	0.11	15.90	5.64	5.22	0.06	3.33	4.45	0.19	0.64
	CJ1 24.76B	53.18	0.27	15.05	5.24	5.42	0.06	4.03	4.32	0.19	0.61
	CJ1 24.85B	52.15	0.19	16.05	5.74	5.08	0.06	3.15	4.51	0.19	0.64
	CJ1 24.86B	51.56	0.05	15.51	6.04	5.24	0.06	3.53	4.34	0.19	0.64
	CJ1 24.91B	53.26	0.45	16.64	5.99	5.13	0.06	3.12	4.65	0.20	0.67
	CJ1 25.00B	52.58	0.19	16.39	5.73	5.05	0.06	2.92	4.57	0.19	0.65
	CJ1 25.08E	51.66	0.21	17.83	6.00	5.17	0.06	2.48	4.88	0.20	0.71
	CJ1 25.11E	51.96	0.25	17.03	5.94	5.25	0.06	2.93	4.68	0.20	0.70
	CJ1 25.14E	50.08	0.16	15.68	6.24	5.80	0.08	4.22	4.35	0.22	0.67
	CJ1 25.56B	52.10	0.15	15.89	5.59	5.22	0.06	3.43	4.44	0.19	0.63
	CJ1 25.60B	52.16	0.21	15.87	5.67	5.13	0.06	3.28	4.44	0.19	0.64
	CJ1 25.60E	46.52	0.11	13.48	5.82	6.82	0.10	6.72	3.78	0.24	0.62
	CJ1 25.62B	57.46	0.25	17.72	5.72	3.77	0.04	0.62	4.98	0.21	0.69
	CJ1 25.69B	53.62	0.23	16.18	5.46	4.98	0.06	2.94	4.54	0.18	0.64
	CJ1 25.72B	53.72	0.22	15.98	5.41	4.97	0.06	3.04	4.47	0.19	0.64
	CJ1 25.72E	50.76	0.08	16.37	6.36	5.13	0.06	3.10	4.55	0.23	0.68
	CJ1 25.92B	52.77	0.13	16.51	5.83	5.15	0.06	3.01	4.60	0.17	0.64
	CJ1 33.10	50.49	0.54	15.61	5.60	5.49	0.07	3.98	4.44	0.22	0.63
	CJ1 33.80	53.50	0.07	15.51	5.90	4.77	0.06	2.90	4.42	0.20	0.66
	CJ1 37.25	50.69	0.08	14.81	6.39	4.32	0.06	2.55	4.29	0.29	0.66
	CJ1 38.40	50.62	0.59	14.18	6.03	4.20	0.05	2.94	4.31	0.61	0.69
	CJ1 39.75	39.07	0.10	12.65	5.26	8.38	0.16	9.84	3.69	0.21	0.52
	CJ1 40.65	54.01	0.18	14.23	5.98	3.61	0.04	1.82	4.39	0.43	0.70
	CJ1 41.80	41.88	0.33	10.24	5.12	7.34	0.12	8.96	3.21	0.54	0.56

		SiO_2 (wt. %)	TiO_2 (wt. %)	Al_2O_3 (wt. %)	Fe_2O_3 (wt. %)	MgO (wt. %)	MnO (wt. %)	CaO (wt. %)	K_2O (wt. %)	Na_2O (wt. %)	P_2O_5 (wt. %)
Average Sauk (all samples)											
		48.25	**0.45**	**16.56**	**5.98**	**4.00**	**0.06**	**6.75**	**3.82**	**0.58**	**0.33**
PAAS Shale Composite Standard (Taylor & McLennan, 1985)											
	PAAS	**62.80**	**1.00**	**18.90**	**6.50**	**2.20**	**0.11**	**1.30**	**3.70**	**1.20**	**0.16**

Table S2: $\delta^{13}C$ and $\delta^{18}O$ measurements from outer detrital belt mudstones. Data for 251 samples of authigenic carbonates from eight outer detrital belt mudstone units of early and middle Cambrian age are shown. Two sample types are present: 1. authigenic cements in mudstones and, 2.concretions. Both sample types show $\delta^{13}C$ values that lie within or very near the range of seawater values for the early and middle Cambrian. The majority of the variation in $\delta^{13}C$ within the data set is stratigraphic, that is, it tracks variation in seawater $\delta^{13}C$ from the early Cambrian (-4.0 - +4.0‰; Maloof et al., 2011) through the middle Cambrian (-4.0 - +1.0‰; Montanez et al., 2000). While some modest influence of organically derived bicarbonate is present in some samples, $\delta^{13}C$ of authigenic carbonates indicates that the primary source of bicarbonate from which the carbonates precipitated was seawater. For these analyses, whole rock powders were dissolved in phosphoric acid and CO_2 evolved was analyzed online by mass spectrometry at Mountain Mass Spectrometry, the University of California, Davis' Stable Isotope facility, and at the University of California, Riverside. Carbon and oxygen isotopic compositions are expressed as permil (‰) deviations from VPDB using the conventional delta notation with a standard deviation no larger than 0.2‰ for both carbon and oxygen. Data for 30 samples of Kaili Formation mudstones was taken from Guo et al. (2010).

Sample	∂13C(VPDB)	∂18O(VPDB)	Sample type	Locality	Age
Kaili Fm.					
41.3 (Guo et al., 2010)	−1.5	−8.9	mudstone	Wuliu-Zengjiayan Section	Cambrian Series 2
42.3 (Guo et al., 2010)	−1.3	−8.7	mudstone	Wuliu-Zengjiayan Section	Cambrian Series 2
43.8 (Guo et al., 2010)	−1.2	−8.6	mudstone	Wuliu-Zengjiayan Section	Cambrian Series 2
44.8 (Guo et al., 2010)	−1.2	−8.3	mudstone	Wuliu-Zengjiayan Section	Cambrian Series 2
47.3 (Guo et al., 2010)	−1.1	−8.7	mudstone	Wuliu-Zengjiayan Section	Cambrian Series 2
49.3 (Guo et al., 2010)	−0.9	−8.8	mudstone	Wuliu-Zengjiayan Section	Cambrian Series 2
50.8 (Guo et al., 2010)	−1.0	−8.4	mudstone	Wuliu-Zengjiayan Section	Cambrian Series 2
53.2 (Guo et al., 2010)	−0.7	−9.2	mudstone	Wuliu-Zengjiayan Section	Cambrian Series 3
54.0 (Guo et al., 2010)	−0.4	−9.2	mudstone	Wuliu-Zengjiayan Section	Cambrian Series 3
54.9 (Guo et al., 2010)	−2.0	−9.6	mudstone	Wuliu-Zengjiayan Section	Cambrian Series 3
55.6 (Guo et al., 2010)	−1.1	−9.0	mudstone	Wuliu-Zengjiayan Section	Cambrian Series 3
57.7 (Guo et al., 2010)	−2.0	−8.3	mudstone	Wuliu-Zengjiayan Section	Cambrian Series 3
59.2 (Guo et al., 2010)	−1.5	−8.6	mudstone	Wuliu-Zengjiayan Section	Cambrian Series 3
61.4 (Guo et al., 2010)	−0.3	−9.3	mudstone	Wuliu-Zengjiayan Section	Cambrian Series 3
61.8 (Guo et al., 2010)	−1.3	−7.1	mudstone	Wuliu-Zengjiayan Section	Cambrian Series 3
62.2 (Guo et al., 2010)	−1.1	−7.5	mudstone	Wuliu-Zengjiayan Section	Cambrian Series 3
63.2 (Guo et al., 2010)	−0.6	−9.2	mudstone	Wuliu-Zengjiayan Section	Cambrian Series 3
63.6 (Guo et al., 2010)	−1.3	−8.4	mudstone	Wuliu-Zengjiayan Section	Cambrian Series 3
64.0 (Guo et al., 2010)	−0.7	−8.1	mudstone	Wuliu-Zengjiayan Section	Cambrian Series 3
64.2 (Guo et al., 2010)	−0.1	−9.9	mudstone	Wuliu-Zengjiayan Section	Cambrian Series 3
64.4 (Guo et al., 2010)	−0.1	−9.4	mudstone	Wuliu-Zengjiayan Section	Cambrian Series 3
64.8 (Guo et al., 2010)	−0.5	−9.4	mudstone	Wuliu-Zengjiayan Section	Cambrian Series 3
65.0 (Guo et al., 2010)	−0.6	−9.1	mudstone	Wuliu-Zengjiayan Section	Cambrian Series 3
65.2 (Guo et al., 2010)	−2.7	−8.4	mudstone	Wuliu-Zengjiayan Section	Cambrian Series 3
65.5 (Guo et al., 2010)	−1.6	−8.4	mudstone	Wuliu-Zengjiayan Section	Cambrian Series 3
66.3 (Guo et al., 2010)	−1.5	−8.9	mudstone	Wuliu-Zengjiayan Section	Cambrian Series 3
66.7 (Guo et al., 2010)	−2.4	−8.9	mudstone	Wuliu-Zengjiayan Section	Cambrian Series 3

Sample	∂¹³C(VPDB)	∂¹⁸O(VPDB)	Sample type	Locality	Age
67.3 (Guo et al., 2010)	–1.0	–9.1	mudstone	Wuliu-Zengjiayan Section	Cambrian Series 3
68.4 (Guo et al., 2010)	–0.6	–8.8	mudstone	Wuliu-Zengjiayan Section	Cambrian Series 3
69.6 (Guo et al., 2010)	–0.8	–9.1	mudstone	Wuliu-Zengjiayan Section	Cambrian Series 3
71.3 (Guo et al., 2010)	–0.6	–9.1	mudstone	Wuliu-Zengjiayan Section	Cambrian Series 3
CK 34	-0.36	-8.09	mudstone	Miaobanpo Section	Cambrian Series 3
CK ELD-1	-2.53	-9.20	mudstone	Miaobanpo Section	Cambrian Series 3
CK-A	-1.00	-7.13	mudstone	Miaobanpo Section	Cambrian Series 3
Marjum Fm.					
WHQ	-0.17	-10.14	mudstone	Upper Marjum Fm., Marjum Pass	Cambrian Series 3
MP	0.03	-10.05	mudstone	Upper Marjum Fm., Marjum Pass	Cambrian Series 3
MJ KK	0.77	-8.72	mudstone	Lower Marjum Fm., Kell's Knolls	Cambrian Series 3
RW	0.83	-8.94	mudstone	Lower Marjum Fm., Red Cliffs Wash	Cambrian Series 3
SG1	0.07	-10.33	mudstone	Lower Marjum Fm., Sponge Gully	Cambrian Series 3
SG2	0.22	-10.40	mudstone	Lower Marjum Fm., Sponge Gully	Cambrian Series 3
MJ1	0.31	-10.30	mudstone	Lower Marjum Fm., Sponge Gully	Cambrian Series 3
MJ13	0.26	-10.42	mudstone	Lower Marjum Fm., Sponge Gully	Cambrian Series 3
MJ21	0.30	-10.34	mudstone	Lower Marjum Fm., Sponge Gully	Cambrian Series 3
MJ47	0.24	-10.40	mudstone	Lower Marjum Fm., Sponge Gully	Cambrian Series 3
MJ68	0.47	-10.43	mudstone	Lower Marjum Fm., Sponge Gully	Cambrian Series 3
BVC D	1.73	-10.32	concretion	Lower Marjum Fm., Marjum Pass	Cambrian Series 3
BVC R	1.44	-10.35	concretion	Lower Marjum Fm., Marjum Pass	Cambrian Series 3
Pierson Cove Fm.					
DMQ 45	-0.60	-10.24	mudstone	Lower Pierson Cove Fm., Drum Mountains	Cambrian Series 3
DMQ 61	-0.76	-10.16	mudstone	Lower Pierson Cove Fm., Drum Mountains	Cambrian Series 3
DMQ 70	-0.68	-10.40	mudstone	Lower Pierson Cove Fm., Drum Mountains	Cambrian Series 3
DMQ1	-0.72	-7.80	mudstone	Lower Pierson Cove Fm., Drum Mountains	Cambrian Series 3
DMQ2	-0.52	-10.64	mudstone	Lower Pierson Cove Fm., Drum Mountains	Cambrian Series 3
DMQ3	-0.46	-10.22	mudstone	Lower Pierson Cove Fm., Drum Mountains	Cambrian Series 3
DMQ4	-0.53	-10.35	mudstone	Lower Pierson Cove Fm., Drum Mountains	Cambrian Series 3
DMQ5	-0.47	-10.28	mudstone	Lower Pierson Cove Fm., Drum Mountains	Cambrian Series 3
DMQ6	-0.51	-10.13	mudstone	Lower Pierson Cove Fm., Drum Mountains	Cambrian Series 3
DMQ7	-0.53	-10.23	mudstone	Lower Pierson Cove Fm., Drum Mountains	Cambrian Series 3
DMQ8	-0.51	-10.27	mudstone	Lower Pierson Cove Fm., Drum Mountains	Cambrian Series 3
Spence Shale Mbr.					
MH5 118	-0.73	-15.25	mudstone	Cycle 5, Miner's Holow	Cambrian Series 3
MH5 126	-1.59	-10.49	mudstone	Cycle 5, Miner's Holow	Cambrian Series 3
CS ON	0.11	-15.12	mudstone	Lower Spence Mbr., Oneida Narrows	Cambrian Series 3
Stephen Fm.					
BPB	-0.20	-14.61	mudstone	Walcott Quarry	Cambrian Series 3

Sample	$\partial^{13}C$(VPDB)	$\partial^{18}O$(VPDB)	Sample type	Locality	Age
OG4	-0.09	-13.96	mudstone	Mt. Stephen	Cambrian Series 3
GPB 124	-0.29	-14.27	mudstone	Walcott Quarry; ROM GPB124	Cambrian Series 3
GPB 125	-0.05	-14.55	mudstone	Walcott Quarry: ROM GPB125	Cambrian Series 3
"thin' Stephen Fm.					
BSG 1033	-0.90	-11.38	mudstone	Stanley Glacier, Cycle 5; ROM 59951	Cambrian Series 3
BSG 1035	0.32	-8.91	mudstone	Stanley Glacier, Cycle 5; ROM 59951	Cambrian Series 3
SG1 27.01	-2.11	-15.71	mudstone	Stanley Glacier, Cycle 5; ROM 59951	Cambrian Series 3
SG1 27.62	-1.91	-12.82	mudstone	Stanley Glacier, Cycle 5; ROM 59951	Cambrian Series 3
SG1 28.37	-1.75	-12.85	mudstone	Stanley Glacier, Cycle 5; ROM 59951	Cambrian Series 3
SG1 29.65	-2.23	-13.21	mudstone	Stanley Glacier, Cycle 5 ; ROM 59951	Cambrian Series 3
SG1 30.0	-1.76	-13.16	mudstone	Stanley Glacier, Cycle 5; ROM 59951	Cambrian Series 3
Wheeler Fm.					
DM311	-0.15	-10.19	mudstone	Upper Wheeler Fm., Drum Mountains	Cambrian Series 3
DMJ16	-0.11	-9.82	mudstone	Upper Wheeler Fm., Drum Mountains	Cambrian Series 3
DMJ17	-0.14	-10.02	mudstone	Upper Wheeler Fm., Drum Mountains	Cambrian Series 3
DMJ20	-0.15	-10.01	mudstone	Upper Wheeler Fm., Drum Mountains	Cambrian Series 3
DMJ28	-0.20	-10.43	mudstone	Upper Wheeler Fm., Drum Mountains	Cambrian Series 3
DMJ31	-0.17	-9.73	mudstone	Upper Wheeler Fm., Drum Mountains	Cambrian Series 3
DMJ34	-0.18	-10.51	mudstone	Upper Wheeler Fm., Drum Mountains	Cambrian Series 3
DMJ36-38	-0.24	-10.65	mudstone	Upper Wheeler Fm., Drum Mountains	Cambrian Series 3
DMJ5	-0.10	-9.63	mudstone	Upper Wheeler Fm., Drum Mountains	Cambrian Series 3
DMJ60	-0.48	-11.45	mudstone	Upper Wheeler Fm., Drum Mountains	Cambrian Series 3
DMM2	0.80	-8.98	mudstone	Upper Wheeler Fm., Drum Mountains	Cambrian Series 3
DMUA	-0.56	-9.42	mudstone	Upper Wheeler Fm., Drum Mountains	Cambrian Series 3
DMUB	-0.05	-9.08	mudstone	Upper Wheeler Fm., Drum Mountains	Cambrian Series 3
SS1	-0.85	-9.75	mudstone	Lower Wheeler Fm., Swasey Spring	Cambrian Series 3
SS2	-0.79	-9.87	mudstone	Lower Wheeler Fm., Swasey Spring	Cambrian Series 3
SS3	-0.80	-9.78	mudstone	Lower Wheeler Fm., Swasey Spring	Cambrian Series 3
WA1 0.07	-0.43	-9.31	mudstone	Upper Wheeler Fm., Wheeler Amphiteater	Cambrian Series 3
WA1 0.10	-0.92	-9.94	mudstone	Upper Wheeler Fm., Wheeler Amphiteater	Cambrian Series 3
WA1 0.37	-0.85	-9.39	mudstone	Upper Wheeler Fm., Wheeler Amphiteater	Cambrian Series 3
WA1 0.49T	-0.31	-9.84	mudstone	Upper Wheeler Fm., Wheeler Amphiteater	Cambrian Series 3
WA1 0.96	-0.73	-9.54	mudstone	Upper Wheeler Fm., Wheeler Amphiteater	Cambrian Series 3
WA1 1.39T	-0.47	-10.04	mudstone	Upper Wheeler Fm., Wheeler Amphiteater	Cambrian Series 3
WA2 2.09	-0.97	-10.48	mudstone	Middle Wheeler Fm., Wheeler Amphiteater	Cambrian Series 3
WA2 2.11	-0.78	-10.68	mudstone	Middle Wheeler Fm., Wheeler Amphiteater	Cambrian Series 3
WA2 3.46	-1.20	-10.48	mudstone	Middle Wheeler Fm., Wheeler Amphiteater	Cambrian Series 3
WA2-2 0.0	-1.95	-12.17	mudstone	Middle Wheeler Fm., Wheeler Amphiteater	Cambrian Series 3
WA2-2 0.1	-1.13	-10.75	mudstone	Middle Wheeler Fm., Wheeler Amphiteater	Cambrian Series 3

Sample	$\partial^{13}C$(VPDB)	$\partial^{18}O$(VPDB)	Sample type	Locality	Age
WA2-2 0.9	-1.10	-10.82	mudstone	Middle Wheeler Fm., Wheeler Amphiteater	Cambrian Series 3
WA2-2 1.5	-1.65	-12.78	mudstone	Middle Wheeler Fm., Wheeler Amphiteater	Cambrian Series 3
WA2-2 1.6	-1.49	-11.53	mudstone	Middle Wheeler Fm., Wheeler Amphiteater	Cambrian Series 3
C1A	-0.29	-10.03	concretion	Lower Wheeler Fm., Marjum Pass	Cambrian Series 3
C1B	-0.39	-9.79	concretion	Lower Wheeler Fm., Marjum Pass	Cambrian Series 3
C1C	-0.28	-10.21	concretion	Lower Wheeler Fm., Marjum Pass	Cambrian Series 3
C1D	-0.97	-10.10	concretion	Lower Wheeler Fm., Marjum Pass	Cambrian Series 3
C1E	-0.52	-10.13	concretion	Lower Wheeler Fm., Marjum Pass	Cambrian Series 3
C3A	-2.21	-10.17	concretion	Lower Wheeler Fm., Marjum Pass	Cambrian Series 3
C3B	-2.05	-10.34	concretion	Lower Wheeler Fm., Marjum Pass	Cambrian Series 3
C3C	-1.86	-10.72	concretion	Lower Wheeler Fm., Marjum Pass	Cambrian Series 3
C3D	-3.04	-9.52	concretion	Lower Wheeler Fm., Marjum Pass	Cambrian Series 3
C3E	-2.09	-10.39	concretion	Lower Wheeler Fm., Marjum Pass	Cambrian Series 3
C3F	-2.99	-9.52	concretion	Lower Wheeler Fm., Marjum Pass	Cambrian Series 3
C4A	-2.45	-10.28	concretion	Lower Wheeler Fm., Marjum Pass	Cambrian Series 3
C4B	-2.31	-10.06	concretion	Lower Wheeler Fm., Marjum Pass	Cambrian Series 3
C6A	-1.26	-10.23	concretion	Lower Wheeler Fm., Marjum Pass	Cambrian Series 3
C6B	-1.82	-10.17	concretion	Lower Wheeler Fm., Marjum Pass	Cambrian Series 3
C6C	-1.78	-9.92	concretion	Lower Wheeler Fm., Marjum Pass	Cambrian Series 3
C6D	-1.81	-10.28	concretion	Lower Wheeler Fm., Marjum Pass	Cambrian Series 3
C6E	-1.83	-10.36	concretion	Lower Wheeler Fm., Marjum Pass	Cambrian Series 3
116A	-2.79	-10.39	concretion	Lower Wheeler Fm., Marjum Pass	Cambrian Series 3
116B	-1.29	-9.65	concretion	Lower Wheeler Fm., Marjum Pass	Cambrian Series 3
116C	-0.65	-10.82	concretion	Lower Wheeler Fm., Marjum Pass	Cambrian Series 3
116D	-0.34	-10.77	concretion	Lower Wheeler Fm., Marjum Pass	Cambrian Series 3
116E	-0.49	-10.94	concretion	Lower Wheeler Fm., Marjum Pass	Cambrian Series 3
116F	-0.60	-10.84	concretion	Lower Wheeler Fm., Marjum Pass	Cambrian Series 3
116G	-0.56	-10.82	concretion	Lower Wheeler Fm., Marjum Pass	Cambrian Series 3
116H	-1.13	-10.82	concretion	Lower Wheeler Fm., Marjum Pass	Cambrian Series 3
116-i	-0.98	-10.79	concretion	Lower Wheeler Fm., Marjum Pass	Cambrian Series 3
116K	-0.55	-10.74	concretion	Lower Wheeler Fm., Marjum Pass	Cambrian Series 3
116L	-0.56	-10.87	concretion	Lower Wheeler Fm., Marjum Pass	Cambrian Series 3
128A	-1.31	-10.83	concretion	Lower Wheeler Fm., Marjum Pass	Cambrian Series 3
128B	-1.16	-10.81	concretion	Lower Wheeler Fm., Marjum Pass	Cambrian Series 3
128C	-0.76	-10.86	concretion	Lower Wheeler Fm., Marjum Pass	Cambrian Series 3
128D	-0.63	-10.87	concretion	Lower Wheeler Fm., Marjum Pass	Cambrian Series 3
128E	-0.54	-10.80	concretion	Lower Wheeler Fm., Marjum Pass	Cambrian Series 3
128F	-0.45	-10.90	concretion	Lower Wheeler Fm., Marjum Pass	Cambrian Series 3
128G	-1.01	-10.85	concretion	Lower Wheeler Fm., Marjum Pass	Cambrian Series 3

Sample	∂^{13}C(VPDB)	∂^{18}O(VPDB)	Sample type	Locality	Age
128H	-1.03	-10.93	concretion	Lower Wheeler Fm., Marjum Pass	Cambrian Series 3
128-i	-0.55	-10.79	concretion	Lower Wheeler Fm., Marjum Pass	Cambrian Series 3
128K	-0.43	-10.89	concretion	Lower Wheeler Fm., Marjum Pass	Cambrian Series 3
128L	-0.64	-10.85	concretion	Lower Wheeler Fm., Marjum Pass	Cambrian Series 3
162A	-1.56	-10.85	concretion	Lower Wheeler Fm., Marjum Pass	Cambrian Series 3
162B	-1.36	-10.79	concretion	Lower Wheeler Fm., Marjum Pass	Cambrian Series 3
162C	-1.21	-10.85	concretion	Lower Wheeler Fm., Marjum Pass	Cambrian Series 3
162D	-0.94	-10.84	concretion	Lower Wheeler Fm., Marjum Pass	Cambrian Series 3
162E	-0.81	-10.96	concretion	Lower Wheeler Fm., Marjum Pass	Cambrian Series 3
162F	-0.57	-10.68	concretion	Lower Wheeler Fm., Marjum Pass	Cambrian Series 3
162G	-0.33	-10.78	concretion	Lower Wheeler Fm., Marjum Pass	Cambrian Series 3
162H	-0.28	-10.93	concretion	Lower Wheeler Fm., Marjum Pass	Cambrian Series 3
162-i	-0.30	-10.75	concretion	Lower Wheeler Fm., Marjum Pass	Cambrian Series 3
162J	-0.96	-10.80	concretion	Lower Wheeler Fm., Marjum Pass	Cambrian Series 3
162K	-0.39	-10.70	concretion	Lower Wheeler Fm., Marjum Pass	Cambrian Series 3
162L	-0.19	-10.62	concretion	Lower Wheeler Fm., Marjum Pass	Cambrian Series 3
164A	-0.69	-10.57	concretion	Lower Wheeler Fm., Marjum Pass	Cambrian Series 3
164B	-0.50	-10.41	concretion	Lower Wheeler Fm., Marjum Pass	Cambrian Series 3
164C	-0.48	-10.38	concretion	Lower Wheeler Fm., Marjum Pass	Cambrian Series 3
164D	-0.59	-10.90	concretion	Lower Wheeler Fm., Marjum Pass	Cambrian Series 3
164E	-0.93	-10.76	concretion	Lower Wheeler Fm., Marjum Pass	Cambrian Series 3
164F	-0.43	-10.41	concretion	Lower Wheeler Fm., Marjum Pass	Cambrian Series 3
164G	-0.64	-10.93	concretion	Lower Wheeler Fm., Marjum Pass	Cambrian Series 3
166A	-2.18	-12.30	concretion	Lower Wheeler Fm., Marjum Pass	Cambrian Series 3
166B	-2.17	-12.53	concretion	Lower Wheeler Fm., Marjum Pass	Cambrian Series 3
166C	-1.85	-10.93	concretion	Lower Wheeler Fm., Marjum Pass	Cambrian Series 3
166D	-0.64	-10.84	concretion	Lower Wheeler Fm., Marjum Pass	Cambrian Series 3
166E	-1.14	-10.74	concretion	Lower Wheeler Fm., Marjum Pass	Cambrian Series 3
166F	-0.45	-12.05	concretion	Lower Wheeler Fm., Marjum Pass	Cambrian Series 3
166G	-0.47	-13.34	concretion	Lower Wheeler Fm., Marjum Pass	Cambrian Series 3
166H	-0.48	-13.62	concretion	Lower Wheeler Fm., Marjum Pass	Cambrian Series 3
166-i	-0.75	-11.07	concretion	Lower Wheeler Fm., Marjum Pass	Cambrian Series 3
166K	-0.66	-11.20	concretion	Lower Wheeler Fm., Marjum Pass	Cambrian Series 3
173A	-0.91	-7.65	concretion	Lower Wheeler Fm., Marjum Pass	Cambrian Series 3
173B	-3.05	-13.69	concretion	Lower Wheeler Fm., Marjum Pass	Cambrian Series 3
173C	-1.46	-10.83	concretion	Lower Wheeler Fm., Marjum Pass	Cambrian Series 3
173D	-0.71	-10.80	concretion	Lower Wheeler Fm., Marjum Pass	Cambrian Series 3
173E	-0.54	-10.82	concretion	Lower Wheeler Fm., Marjum Pass	Cambrian Series 3
173F	-0.55	-10.85	concretion	Lower Wheeler Fm., Marjum Pass	Cambrian Series 3

Sample	∂13C(VPDB)	∂18O(VPDB)	Sample type	Locality	Age
173G	-0.37	-10.72	concretion	Lower Wheeler Fm., Marjum Pass	Cambrian Series 3
173H	-0.31	-10.77	concretion	Lower Wheeler Fm., Marjum Pass	Cambrian Series 3
173-i	-2.91	-11.66	concretion	Lower Wheeler Fm., Marjum Pass	Cambrian Series 3
173K	-0.56	-10.68	concretion	Lower Wheeler Fm., Marjum Pass	Cambrian Series 3
173L	-0.69	-10.60	concretion	Lower Wheeler Fm., Marjum Pass	Cambrian Series 3
181A	-1.10	-12.29	concretion	Lower Wheeler Fm., Marjum Pass	Cambrian Series 3
181B	-1.02	-11.55	concretion	Lower Wheeler Fm., Marjum Pass	Cambrian Series 3
181C	-0.92	-11.38	concretion	Lower Wheeler Fm., Marjum Pass	Cambrian Series 3
181D	-0.93	-11.45	concretion	Lower Wheeler Fm., Marjum Pass	Cambrian Series 3
181E	-1.25	-10.89	concretion	Lower Wheeler Fm., Marjum Pass	Cambrian Series 3
181F	-0.62	-13.32	concretion	Lower Wheeler Fm., Marjum Pass	Cambrian Series 3
181G	-0.49	-12.93	concretion	Lower Wheeler Fm., Marjum Pass	Cambrian Series 3
185A	-1.61	-10.80	concretion	Lower Wheeler Fm., Marjum Pass	Cambrian Series 3
185B	-1.61	-10.83	concretion	Lower Wheeler Fm., Marjum Pass	Cambrian Series 3
185C	-1.22	-10.89	concretion	Lower Wheeler Fm., Marjum Pass	Cambrian Series 3
185D	-0.59	-10.53	concretion	Lower Wheeler Fm., Marjum Pass	Cambrian Series 3
185E	-0.54	-10.79	concretion	Lower Wheeler Fm., Marjum Pass	Cambrian Series 3
185F	-0.48	-10.84	concretion	Lower Wheeler Fm., Marjum Pass	Cambrian Series 3
185G	0.08	-10.69	concretion	Lower Wheeler Fm., Marjum Pass	Cambrian Series 3
185H	-0.78	-10.75	concretion	Lower Wheeler Fm., Marjum Pass	Cambrian Series 3
185-i	-3.07	-14.02	concretion	Lower Wheeler Fm., Marjum Pass	Cambrian Series 3
185K	-2.94	-12.90	concretion	Lower Wheeler Fm., Marjum Pass	Cambrian Series 3
185L	-0.71	-10.70	concretion	Lower Wheeler Fm., Marjum Pass	Cambrian Series 3
Yu'anshan Fm.					
12.96 E3	-3.02	-8.12	mudstone	Borehole, Haikou, Yunnan	Cambrian Series 2
15.26 E	-2.92	-7.88	mudstone	Borehole, Haikou, Yunnan	Cambrian Series 2
15.28 B	-2.16	-6.63	mudstone	Borehole, Haikou, Yunnan	Cambrian Series 2
21.27 B	-2.40	-6.98	mudstone	Borehole, Haikou, Yunnan	Cambrian Series 2
22.25 B	-2.55	-7.46	mudstone	Borehole, Haikou, Yunnan	Cambrian Series 2
23.30 E1	-3.12	-8.51	mudstone	Borehole, Haikou, Yunnan	Cambrian Series 2
23.30 E2	-3.20	-8.85	mudstone	Borehole, Haikou, Yunnan	Cambrian Series 2
23.33 B1	-2.53	-7.19	mudstone	Borehole, Haikou, Yunnan	Cambrian Series 2
23.33 B2	-2.57	-7.40	mudstone	Borehole, Haikou, Yunnan	Cambrian Series 2
23.37 B1	-2.49	-7.31	mudstone	Borehole, Haikou, Yunnan	Cambrian Series 2
23.40 E1	-2.59	-7.35	mudstone	Borehole, Haikou, Yunnan	Cambrian Series 2
23.40 E2	-2.80	-7.75	mudstone	Borehole, Haikou, Yunnan	Cambrian Series 2
23.40 B1	-2.45	-7.26	mudstone	Borehole, Haikou, Yunnan	Cambrian Series 2
23.43 E1	-2.48	-7.20	mudstone	Borehole, Haikou, Yunnan	Cambrian Series 2
23.43 B1	-2.41	-7.28	mudstone	Borehole, Haikou, Yunnan	Cambrian Series 2

Sample	$\partial^{13}C$(VPDB)	$\partial^{18}O$(VPDB)	Sample type	Locality	Age
23.46 E1	-2.26	-6.87	mudstone	Borehole, Haikou, Yunnan	Cambrian Series 2
23.51 E1	-2.35	-6.93	mudstone	Borehole, Haikou, Yunnan	Cambrian Series 2
23.51 E11	-2.34	-6.98	mudstone	Borehole, Haikou, Yunnan	Cambrian Series 2
23.51 B11	-2.50	-7.56	mudstone	Borehole, Haikou, Yunnan	Cambrian Series 2
23.51 E21	-2.12	-6.60	mudstone	Borehole, Haikou, Yunnan	Cambrian Series 2
23.57 E1	-2.44	-7.22	mudstone	Borehole, Haikou, Yunnan	Cambrian Series 2
23.60 E1	-1.93	-6.44	mudstone	Borehole, Haikou, Yunnan	Cambrian Series 2
23.60 B1	-1.96	-7.27	mudstone	Borehole, Haikou, Yunnan	Cambrian Series 2
23.91 B1	-2.39	-7.21	mudstone	Borehole, Haikou, Yunnan	Cambrian Series 2
23.92 S	-3.94	-9.51	mudstone	Borehole, Haikou, Yunnan	Cambrian Series 2
24.12 B	-2.18	-6.71	mudstone	Borehole, Haikou, Yunnan	Cambrian Series 2
24.22 B	-2.02	-6.45	mudstone	Borehole, Haikou, Yunnan	Cambrian Series 2
24.62 B	-2.33	-6.90	mudstone	Borehole, Haikou, Yunnan	Cambrian Series 2
24.70 B	-2.65	-7.53	mudstone	Borehole, Haikou, Yunnan	Cambrian Series 2
24.76 B	-2.73	-7.56	mudstone	Borehole, Haikou, Yunnan	Cambrian Series 2
24.85 B	-2.70	-7.37	mudstone	Borehole, Haikou, Yunnan	Cambrian Series 2
24.91 B	-2.34	-6.56	mudstone	Borehole, Haikou, Yunnan	Cambrian Series 2
24.91 E	-2.26	-6.49	mudstone	Borehole, Haikou, Yunnan	Cambrian Series 2
25.00 B	-2.53	-7.23	mudstone	Borehole, Haikou, Yunnan	Cambrian Series 2
25.08 E	-2.00	-6.38	mudstone	Borehole, Haikou, Yunnan	Cambrian Series 2
25.11 E2	-2.28	-6.79	mudstone	Borehole, Haikou, Yunnan	Cambrian Series 2
25.11 B	-2.48	-7.21	mudstone	Borehole, Haikou, Yunnan	Cambrian Series 2
25.14 B	-2.54	-7.29	mudstone	Borehole, Haikou, Yunnan	Cambrian Series 2
25.56 B	-2.63	-7.08	mudstone	Borehole, Haikou, Yunnan	Cambrian Series 2
25.60 B	-2.53	-6.94	mudstone	Borehole, Haikou, Yunnan	Cambrian Series 2
25.60 E	-3.32	-8.40	mudstone	Borehole, Haikou, Yunnan	Cambrian Series 2
25.69 B	-2.49	-6.95	mudstone	Borehole, Haikou, Yunnan	Cambrian Series 2
25.72 B	-1.54	-5.50	mudstone	Borehole, Haikou, Yunnan	Cambrian Series 2
25.72 E	-1.90	-5.81	mudstone	Borehole, Haikou, Yunnan	Cambrian Series 2
25.73 B	-1.96	-6.14	mudstone	Borehole, Haikou, Yunnan	Cambrian Series 2
25.75 B	-2.48	-6.90	mudstone	Borehole, Haikou, Yunnan	Cambrian Series 2
25.92 B	-2.43	-6.78	mudstone	Borehole, Haikou, Yunnan	Cambrian Series 2
32.00 B	-2.74	-7.31	mudstone	Borehole, Haikou, Yunnan	Cambrian Series 2
33.10 B	-2.90	-7.81	mudstone	Borehole, Haikou, Yunnan	Cambrian Series 2
33.80 B	-2.93	-7.43	mudstone	Borehole, Haikou, Yunnan	Cambrian Series 2
38.40 B	-1.89	-7.95	mudstone	Borehole, Haikou, Yunnan	Cambrian Series 2

Table S3: Raw stratigraphic/lithologic data. Stratigraphic and sedimentologic data from North America, binned into Phanerozoic epochs. Age given in Myr ago, carbonate flux given in km^3/Myr, area given in km^2. "Units" refers to number of lithostratigraphic rock units in Macrostrat (macrostrat.org). Carbonate mass flux given in cubic kilometers per million years.

interval_name	age_bot-tom	n_glauc_units	n_sed_units	n_carb_units	carb_mass_flux	n_col_on_sed	n_col_on_base	area_on_base	n_feldspathic
Holocene	0.0117	0	733	0	72.08032	106	0	0	0
Pleistocene	1.806	1	1213	4	10100.26317	373	5	62819.883	6
Pliocene	5.332	8	442	4	16899.78474	148	1	3890.494	9
Miocene	23.03	12	841	17	28844.449	177	7	60970.62	21
Oligocene	33.9	10	388	57	31402.70313	82	5	54907.906	8
Eocene	55.8	40	900	78	59683.32753	104	30	242916.912	22
Paleocene	65.5	27	457	30	23469.54304	123	22	141195.09	13
Late Cretaceous	99.6	57	1618	137	27301.24145	149	34	260058.653	22
Early Cretaceous	145.5	4	1172	174	26984.40155	187	31	263005.045	15
Late Jurassic	161.2	4	485	55	22482.31418	75	39	313005.032	6
Middle Jurassic	175.6	1	380	43	10276.64822	85	10	200966.288	5
Early Jurassic	199.6	0	246	12	1849.041585	65	7	91916.348	5
Late Triassic	228	0	387	76	13959.11927	75	25	261636.352	8
Middle Triassic	245	1	172	27	5397.669442	48	12	161420.176	4
Early Triassic	251	1	154	23	17873.6813	85	4	39090.68	0
Late Permian	260.4	1	119	20	8391.855409	8	1	2777.046	0
Early Permian	299	1	751	285	47775.87155	105	13	344301.326	10
Pennsylvanian	318.1	1	1646	524	82912.36754	170	25	841238.254	13
Mississippian	359.2	15	1658	710	57833.32375	187	25	597057.121	8
Late Devonian	385.3	2	943	237	45920.42736	158	10	132230.62	4
Middle Devonian	397.5	1	776	365	87789.15082	108	11	559227.296	3
Early Devonian	416	0	631	286	57428.77984	105	5	92610.028	3
Pridoli	418.7	0	395	186	71479.15759	7	1	3928.627	2
Ludlow	422.9	0	489	231	86501.08843	24	2	37939.031	2
Wenlock	428.2	0	511	249	60076.34687	23	4	120858.155	3
Llandovery	443.7	1	603	291	58240.82379	127	12	194178.87	8
Late Ordovician	460.9	0	1455	835	97548.27645	150	21	1083456.767	4
Middle Ordovician	471.8	0	509	259	55384.17154	121	19	352048.923	5
Early Ordovician	488.3	4	603	412	91855.00242	43	35	805049.818	5
Late Cambrian	501	46	885	452	115115.4861	45	121	2557757.997	18
Middle Cambrian	513	9	564	268	85858.55508	37	64	1819322.817	11
Early Cambrian	542	4	362	95	15584.02318	41	73	1025951.648	18

REFERENCES CITED

Avigad, D. et al., Mass-production of Cambro-Ordovician quartz-rich sandstone as a consequence of chemical weathering of Pan-African terranes: environmental implications. Earth Planet. Sci. Lett. 240, 818-826 (2005).

Brasier, M.D. The Lower Cambrian transgression and glauconite-phosphate facies in western Europe. J. Geol. Soc. London 137, 695-703 (1980).

Guo, Q., Strauss, H., Liu, C., Zhao, Y., Yang, X., Peng, J., Yang, H., 2010. A negative carbon excursion defines the boundary from Cambrian Series 2 to Cambrian Series 3 on the Yangtze Platform, South China. Palaeogeography Palaeoclimatology Palaeoecology 285, 143–151.

Johnson, D. M., Hooper, P. R., and Conrey, R. M., 1999, XRF analysis of rocks and minerals for major and trace elements on a single low dilution Li-tetraborate fused bead: Advances in X-ray Analysis, 41, 843–867.

Laird, M.G. in Geological evolution of Antarctica (Cambridge, Cambridge, 1991), pp. 177-186.

Liñán, E., Gozalo, R., Palacios, T., Gámez Vinaned, J.A., Ugidos, J.M. & Mayoral, E. 2002. Cambrian, 17 29. In Gibbons, W. & Moreno, T. (eds) The Geology of Spain. The Geological Society, London.

Maloof, A.C., Porter, S.M., Moore, J.L., Dudas, F.O., Bowring, S.A., Higgins, J.A., Fike, D.A., and Eddy, M.P., 2010, The earliest Cambrian record of animals and ocean geochemical change. Geol. Soc. Am. Bull. 122, 1731-1774.

Meng, X., Ge, M., and Tucker, M.E., 1997, Sequence stratigraphy, sea-level changes and depositional systems in the Cambro-Ordovician of the North China carbonate platform, Sedimentary Geology 114, 189-222.

Miller, E.L., Kuznetsov, N., Soboleva, A., Udoratina, O., Grove, M.J., and Gehrels, G., 2011 et al., Baltica in the Cordillera? Geology 39, 791-794.

Montañez I.P., Osleger D.A., Banner J., Mack L.E., & Musgrove M., 2000, Evolution of the Sr and C isotope composition of Cambrian Oceans, GSA today 10:1-7.

Pettijohn, F.J., Potter, P.E., and Siever, R., 1987, Sand and Sandstone. Springer Verlag: New York, 572 p.

Sears, J.W. & Price, R.A. Tightening the Siberian connection to western Laurentia. Geol. Soc. Am. Bull. 115, 943-953 (2003).

Taylor, S.R., and McLennan, S.M., 1985, The Continental Crust: its Composition and Evolution. Blackwell: London, 312 p.